

DRetHTR: Linear-Time Decoder-Only Retentive Network for Handwritten Text Recognition

Changhun Kim¹, Martin Mayr¹, Thomas Gorges¹, Fei Wu¹, Mathias Seuret¹,
Andreas Maier¹, Vincent Christlein¹

¹ Pattern Recognition Lab, Friedrich-Alexander-Universität Erlangen-Nürnberg, Germany

ABSTRACT

State-of-the-art handwritten text recognition (HTR) systems commonly use Transformers, whose growing key-value (KV) cache makes decoding slow and memory-intensive. We introduce DRetHTR, a decoder-only model built on Retentive Networks (RetNet). Compared to an equally sized decoder-only Transformer baseline, DRetHTR delivers 1.6–1.9× faster inference with 38–42% less memory usage, without loss of accuracy. By replacing softmax attention with softmax-free retention and injecting multi-scale sequential priors, DRetHTR avoids a growing KV cache: decoding is linear in output length in both time and memory. To recover the local-to-global inductive bias of attention, we propose layer-wise gamma scaling, which progressively enlarges the effective retention horizon in deeper layers. This encourages early layers to model short-range dependencies and later layers to capture broader context, mitigating the flexibility gap introduced by removing softmax. Consequently, DRetHTR achieves best reported test character error rates of 2.26% (IAM-A, en), 1.81% (RIMES, fr), and 3.46% (Bentham, en), and is competitive on READ-2016 (de) with 4.21%. This demonstrates that decoder-only RetNet enables Transformer-level HTR accuracy with substantially improved decoding speed and memory efficiency.

Index Terms— Handwritten Text Recognition (HTR), Retentive Network (RetNet), Efficient inference, Decoder-only architecture, Image–text fusion

1. INTRODUCTION

Digitized documents permeate healthcare, insurance, government, and finance, yet a vast body of handwritten content remains locked in archives and libraries worldwide. Handwritten Text Recognition (HTR) addresses these challenges by teaching machines to decode handwriting: platforms such as Transkribus [1] have demonstrated the practical impact of large-scale transcription for historians, genealogists, and the digital humanities, accelerating scholarship and public access to archival records. Beyond cultural heritage, modern administrative workflows across sectors have also been automated by HTR, saving enormous manual labor and improving productivity [2]. HTR is a pattern recognition problem over visual sequences: the system must map an input image to a character sequence while leveraging linguistic regularities in context.

Initial approaches such as Hidden Markov Models (HMMs) [3] transitioned to more complex architectures like Bidirectional Long Short-Term Memory (BiLSTM). However, distinguishing between similar characters is still challenging without context knowledge, which is usually handled by external language models [4].

DRetHTR with Layer-wise Gamma Scaling

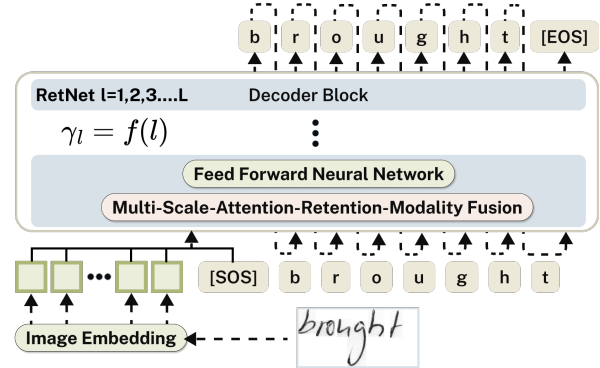


Fig. 1. Decoder-only RetNet architecture that fuses the image and text in the Decoder

Popular line-based approaches [5,6] use a combination of Convolutional Neural Networks (CNNs) and Recurrent Neural Networks (RNNs), trained through the Connectionist Temporal Classification (CTC) loss [7]. This enables alignment between input image and output character sequences without predefined character segmentation. However, limitations such as enforcing strict input-output sequence alignment and limiting the output lengths remain. This motivates the usage of sequence-to-sequence architectures, especially Transformers [8], allowing for unrestricted sequence length and the use of contextual cues.

DTrOCR [9] was introduced as an effective decoder-only architecture for HTR, surpassing previous models by leveraging the pre-trained GPT-2 [10], which provides robust natural language understanding. However, Transformer self-attention must form (and typically store) an $N \times N$ attention map for a sequence of length N , making long sequences costly. In contrast, RNNs decode with constant per-step cost and long-sequence memory that grows only linearly with N , but they lack Transformer-style parallel training.

Retentive Networks (RetNets) address this trade-off by combining parallel training with a softmax-free *retention* mechanism that admits a recurrent form at inference [11]. This enables constant-cost decoding per step with linear long-sequence memory, while maintaining competitive performance, making RetNet an attractive foundation for efficient HTR.

To harness these advantages for HTR, we introduce DRetHTR, a decoder-only RetNet tailored to line-level handwriting that achieves linear-time, linear-memory decoding. At the decoder input, DRetHTR employs an *Attention-Retention Modality Fusion* (ARMF) layer that aligns image and text tokens and provides a *modality-partitioned interface*: image-key interactions use stan-

Corresponding author: changhun.kim@fau.de
Code: <https://github.com/Kimchangheon/DRetHTR>

dard attention for alignment, while text-key interactions use *causal retention* with lower-triangular decay matrix D . To recover the local-to-global inductive bias typically provided by softmax attention, we propose *layer-wise γ scaling* for retention: shallow layers use smaller decay factors to emphasize local dependencies, while deeper layers increase the decay to aggregate broader context. Our ablation study confirms that this schedule matches a Transformer’s CER while preserving linear-time, linear-memory decoding. Under a unified evaluation protocol on IAM [12], RIMES [13], READ-2016 [14], and *Bentham* [15], DRetHTR delivers competitive accuracy with efficiency gains of 1.6–1.9× faster inference and 38–42 % lower memory.

The paper is structured as follows. Section 2 reviews related work on HTR architectures. Section 3 provides background on RetNet and its variants. Section 4 presents DRetHTR, including ARMF and layer-wise γ scaling. Section 5 reports quantitative and qualitative results, including ablations. Section 6 and Section 7 discuss limitations and future work, and Section 8 concludes.

2. RELATED WORK

In the early days of HTR, classical machine learning models such as support vector machines (SVM) and k-Nearest Neighbors (k-NN) were widely used. These methods relied on hand-crafted features extracted from geometric, statistical, or polar-transformed representations of text images. Similarly, Farah *et al.* [16] use a parallel combination of k-NN, fuzzy k-NN, and neural networks to recognize Arabic words with a 96 % accuracy rate. Despite good single-character performance, these methods require tedious segmentation of line images into individual characters or strokes.

HMMs use the sliding window technique to extract a sequence of feature vectors from an entire line of text without needing pre-segmented data. Plotz *et al.* [3] emphasized that HMMs perform implicit alignment between input features and target sequences using the Viterbi decoding. The dominance of RNNs in handwriting recognition was enabled by the introduction of the CTC loss function [7]. Moreover, MDLSTMs [17, 18], Neural Network Language Models [19], RWGD [20], and other approaches [21, 22] have notably improved HTR performance.

Recent developments introduced Transformer-based approaches, significantly enhancing parallel processing, scalability, and global dependency modeling. Notable methods include NRTTR [23], fully Transformer-based architectures by Kang *et al.* [24], and hybrid Transformer-CTC models [25, 26]. For diplomatic transcription in low-data environments, Mayr *et al.* [27] made practical modifications to a Transformer encoder-decoder to bypass the length constraints of CTC. In parallel, several works report that pairing a Transformer decoder with a CTC auxiliary branch on the encoder—or leveraging CTC during decoding—improves data efficiency and recognition accuracy [28–30].

Large-scale pre-trained families, notably TrOCR and DTrOCR, leverage foundational Transformer language models and achieve state-of-the-art accuracy [9, 31]. TrOCR is an end-to-end encoder-decoder that couples a ViT/BEiT-style image encoder with a RoBERTa-initialized text Transformer decoder [31]. By contrast, DTrOCR pushes toward a decoder-only design: images are patch-tokenized and fed to a Transformer decoder initialized from GPT-2, which then autoregressively generates the transcription [9, 10]. This simplification exploits strong language priors and removes encoder-decoder cross-attention, yet it still inherits the quadratic cost of softmax self-attention at decoding time.

3. RETENTIVE NETWORKS – BACKGROUND

Transformer’s self-attention enables fully parallel training; during autoregressive decoding, however, standard implementations maintain a Key-Value (KV) cache that grows linearly with generated length, motivating research on effective KV cache management architectures [32]. RetNet replaces the growing KV cache with a compact recurrent state. Its retention mechanism bridges attention and recurrence: training stays fully parallel, while inference runs as a constant-time recurrence. Retention pursues the same effect as self-attention by circumventing the softmax operation, which prohibits the compatible recurrent representation of self-attention, through the use of a temporal prior decay matrix. The intuitive mathematical compatibility between the parallel form and the recurrent form is explained in A.

From self-attention to retention Let $X \in \mathbb{R}^{N \times d_{\text{model}}}$ be a length- N sequence. A Transformer maps X to $Q = XW_Q$, $K = XW_K$, $V = XW_V$ with $W_Q, W_K, W_V \in \mathbb{R}^{d_{\text{model}} \times d_{\text{model}}}$ and computes $\text{Attn}(X) = \text{softmax}\left(\frac{QK^\top}{\sqrt{d_k}}\right)V$.

Retention: parallel training, recurrent inference In the *parallel (training) form*, retention augments Q and K with per-position complex phases

$$Q = (XW_Q) \odot \Theta, \quad K = (XW_K) \odot \bar{\Theta}, \quad V = XW_V. \quad (1)$$

where \odot is element-wise multiplication, $\bar{\Theta}$ is the complex conjugate of Θ , and the n -th row of Θ is $\Theta_n = e^{i n \theta}$ for position index $n \in \{1, \dots, N\}$. A lower-triangular decay matrix $D \in \mathbb{R}^{N \times N}$ applies a causal, exponential prior

$$D_{nm} = \begin{cases} \gamma^{n-m}, & n \geq m, \\ 0, & n < m, \end{cases} \quad (2)$$

with n the query index, m the key index, and $\gamma \in (0, 1)$ the decay factor. The parallel retention is then

$$\text{Retention}(X) = (QK^\top \odot D)V. \quad (3)$$

Intuitively, D plays the role of a softmax-free, hand-crafted inductive bias that emphasizes recent context while remaining fully parallelizable for training over $n = 1, \dots, N$.

In the *recurrent (inference) form*, the same operator collapses to a constant-time update that no longer needs a growing KV cache. Defining a state $S_n \in \mathbb{C}^{d_{\text{model}} \times d_{\text{model}}}$ at step n ,

$$S_n = \gamma S_{n-1} + k_n^\top v_n, \quad \text{Retention}(x_n) = q_n S_n. \quad (4)$$

where q_n, k_n, v_n are the n -th rows of Q, K, V . This yields $O(1)$ per-token computation and $O(N)$ total memory for a length- N sequence, while Transformers require $O(N)$ per-token time from the growing KV cache and $O(N^2)$ memory overall. A summary of parallelism, inference cost, and memory is shown in Tables 1 and 2. Compared with a KV-cached Transformer, RetNet’s recurrent form is more effective when the model width d is smaller than the sequence length N .

Data-dependent decay (Gated Retention) Gated Retention (gRet) [33] improves upon RetNet [11] by introducing a data-dependent gating mechanism instead of fixed gamma values over the different data samples. Based on the input data, the model can

Table 1. Comparison of model architectures by parallelization, inference cost, memory complexity, and performance.

Architectures	Parallelized training	Inference Cost	Long-Seq Memory	Performance
Transformer	✓	$O(N)$	$O(N^2)$	✓✓
RetNet	✓	$O(1)$	$O(N)$	✓✓
RNN	✗	$O(1)$	$O(N)$	✓

Table 2. Computational costs of different inference forms. RetNet’s recurrent form is more effective than the KV-cached Transformer when model dimension d is less than sequence length n (derivation in Supplementary Materials, B).

Form	Total Computations	Asymptotic Complexity
Vanilla Form	$2n^2d + n^2 - 1 + n(d-1)$	$\mathcal{O}(n^2d)$
Key-Value Cached	$2dn + 2(n-1)$	$\mathcal{O}(nd)$
Recurrent Form	$2d^2 + d - 1$	$\mathcal{O}(d^2)$

automatically learn how the influence of preceding tokens decays as their distance increases, while preserving a recurrent representation. In gRet, γ and D are defined as follows:

$$\gamma = \text{sigmoid}(XW_\gamma)^{1/\tau}, \quad D_{nm} = \begin{cases} \prod_{i=m+1}^n \gamma_i, & n \geq m, \\ 0, & n < m, \end{cases} \quad (5)$$

Here, the temperature τ controls decay sharpness by pushing γ_i toward 1: larger τ slows decay and lengthens memory, whereas smaller τ steepens decay and emphasizes local dependencies; following YOCO [33] we use $\tau = 16$. As in RetNet, a sigmoid value $\gamma \in (0, 1)$ is applied iteratively as a product over the intermediate positions between two tokens, determined by the distance $|n - m|$. This means that the closer the tokens are to each other, the stronger their dependency; conversely, the farther apart they are, the weaker the dependency becomes.

Bi-directional retention for vision RMT [34] incorporates spatial priors into Vision Transformers. RMT builds upon the original retention mechanism by first adapting it to a bi-directional form and subsequently enhancing it with a Manhattan distance-based spatial decay. BiRetention becomes suitable for images as it moves from unidirectional to bidirectional decay. BiRetention is expressed as:

$$\text{BiRetention}(X) = (QK^\top \odot D^{\text{Bi}}) V, \quad D_{nm}^{\text{Bi}} = \gamma^{|n-m|}. \quad (6)$$

4. METHODOLOGY

4.1. DRetHTR Architecture

Our proposed DRetHTR architecture builds upon the Retentive Network with a decoder-only architecture. A key adaptation involves fusing image and text embeddings within the decoder. For image–text fusion, only the parallel form is needed even during inference, so we reintroduce softmax to provide additional nonlinearity and effectively capture relationships among image tokens and between image and text tokens. For inter-text dependencies, we incorporate a temporal prior with a layer-wise scaled gamma value instead of softmax, enabling linearizability during inference.

4.1.1. Image Embedding Module

Instead of the default patch embedding, we use EfficientNetV2 [35] as the image embedder to leverage its feature extraction capability. The ImageNet-1K pre-trained weights [36] are loaded, and the classifier part is removed so that only the feature map is extracted. During training, dropout with a probability of 0.3 is applied after each activation function across all layers. The inclusion of dropout helps the model’s generalization to adapt to the handwriting domain by alleviating overfitting to the features initially learned from ImageNet. Furthermore, to obtain more spatial information for sequence processing, the stride along width of the first convolutional layer is modified from 2 to 1. Once we obtain the 3-dimensional visual feature F with a shape corresponding to $(c_{\text{visual}}, h_{\text{visual}}, w_{\text{visual}})$, where c_{visual} is the number of channels, and $h_{\text{visual}}, w_{\text{visual}}$ represent the height and width of the feature map, it is reshaped into $(w_{\text{visual}}, c_{\text{visual}} \times h_{\text{visual}})$. Through a fully connected layer, it is then transformed into embedding E of shape $(w_{\text{visual}}, d_{\text{model}})$, where d_{model} is a predefined input dimension of the decoder. Finally, the visual feature embedding is added with a learnable positional encoding, initialized with random weights. This visual feature embedding E is considered as a sequence of w_{visual} image tokens, each of dimension d_{model} .

4.1.2. Text Embedding Module

The transcriptions of handwriting images are tokenized at character level. The character map consists of $V = |\mathcal{C}|$ unique characters in the dataset and the special tokens [SOS], [EOS], and [PAD]. According to the maximum length of the transcriptions in the dataset, shorter text transcriptions are padded. Finally, the input text embeddings are represented as T of shape $(\max(l_{\text{text}}), d_{\text{model}})$, where $\max(l_{\text{text}})$ is the fixed sequence length after padding, and d_{model} is the model dimension. Sinusoidal positional encoding is added to the embeddings to provide the model with information about the order of tokens within the sequence.

4.1.3. DRetHTR Decoder

After attaining the image and text tokens from their respective embedders, they are concatenated into a single sequence and passed to the RetNet decoder. The decoder consists of L identical layers stacked on each other. Unlike encoder-decoder architectures, this design omits cross-attention. Instead, modality fusion is achieved solely within the retention layer, adapted as Attention-Retention Modality Fusion (ARMF), a mixture of multi-head attention and multi-scale retention. The architecture comprises two sub-layers: ARMF and Position-wise Feed-Forward (PFF). Both sub-layers are surrounded by residual connections [37], with layer normalization [38] applied afterward. To accommodate residual connections, all sub-layers and embedding layers are designed to output the same dimension of d_{model} . The PFF consists of two linear layers, GELU for smooth non-linearity and a dropout layer to improve generalization.

4.1.4. Attention-Retention Modality Fusion (ARMF)

The limitation of full self-attention over concatenated image–text tokens is a growing KV cache and incurring $O(N)$ per-token decoding. In contrast, applying full retention to all tokens yields $O(1)$ decoding but weakens accuracy by limiting flexible image–text coupling. Therefore, we introduce ARMF, which resolves this by using retention only for the autoregressive text stream—where recurrence is needed—while keeping softmax attention for image–image and image–text interactions. Image keys and values (of length N_I) are

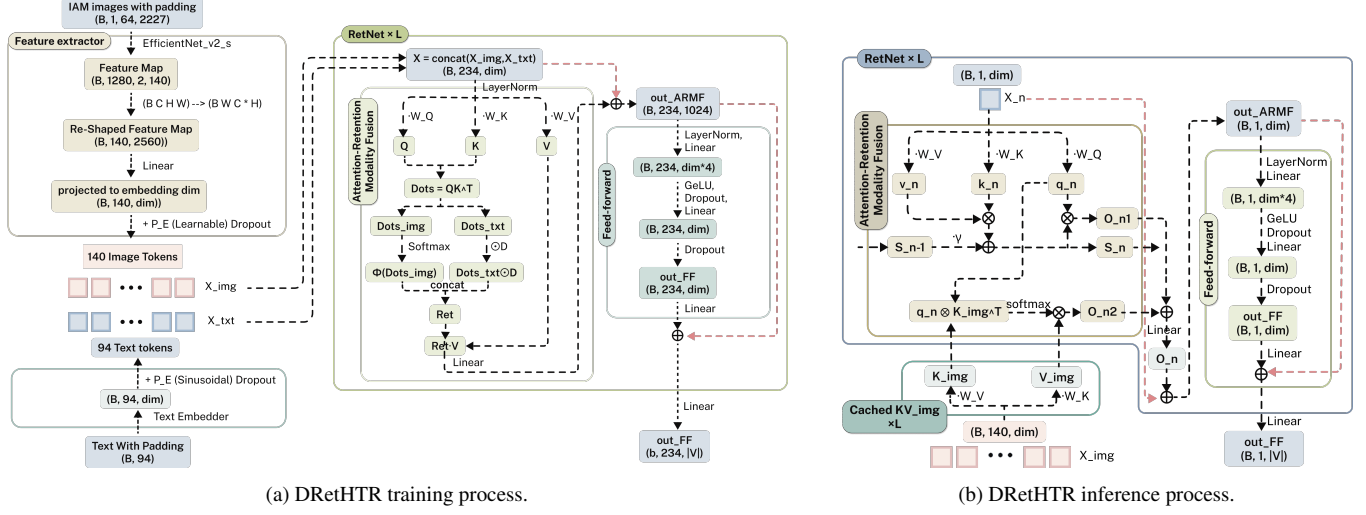


Fig. 2. Illustration of the DRetHTR training and inference processes: **(a)** training; **(b)** inference. ARMF mixes softmax (image) + retention (text) without breaking recurrence.

computed once in parallel and text stream is processed recurrently, so cross-modal softmax does not introduce a KV cache that grows with N_T , preserving RetNet's $O(1)$ decoding with respect to generated text length.

The Parallel Representation of ARMF. As shown in Fig. 2, the ARMF layer is:

$$\begin{aligned}
 X &= \begin{bmatrix} X_{\text{img}} \\ X_{\text{text}} \end{bmatrix} \in \mathbb{R}^{N \times d_{\text{model}}}, \quad N = N_I + N_T \\
 Q &= XW_Q, \quad K = XW_K, \quad V = XW_V \\
 \text{Dots} &= \frac{QK^T}{\sqrt{d_k}} = \left[\begin{array}{cc} \text{Dots}_{\text{img}} \in \mathbb{R}^{N \times N_I} & \text{Dots}_{\text{text}} \in \mathbb{R}^{N \times N_T} \end{array} \right] \\
 D_{ij} &= \begin{cases} 0, & i < N_I, \\ \gamma^{i-N_I-j}, & i \geq N_I, j \leq i - N_I \\ 0, & i \geq N_I, j > i - N_I \end{cases} \\
 \text{Ret} &= \left[\begin{array}{cc} \text{softmax}(\text{Dots}_{\text{img}}) & \text{Dots}_{\text{text}} \odot D \end{array} \right] \\
 \text{ARMF}(X) &= \text{Ret} V \in \mathbb{R}^{N \times d_{\text{model}}}.
 \end{aligned} \tag{7}$$

Where X is the given input sequence. N_I and N_T are the numbers of image and text tokens, respectively. $W_Q, W_K, W_V \in \mathbb{R}^{d_{\text{model}} \times d_{\text{model}}}$ are learnable weights. $D \in \mathbb{R}^{N \times N_T}$ is a dependency mask that prevents image queries from attending to text keys, while, for text queries, it applies causal, exponentially decayed dependence over text keys.

Here, the reintroduced softmax does not prevent the recurrent representation, since computation for all image tokens in the inference phase is inherently parallelized. Softmax operates row-wise, so when a new text token q_n attends the full image length K_{img} and V_{img} , attention with softmax can be computed solely for q_n , independent of previous tokens q_1, q_2, \dots, q_{n-1} . Therefore, we can seamlessly expand the recurrent representation for concatenated image-text input, maintaining compatibility without any collapse.

The Recurrent Representation of ARMF As shown in Figure 2b, ARMF can also be computed recurrently during inference. Unlike conventional retention mechanisms, q_n must pay attention not only to the text tokens but also to the relevant image tokens. To achieve this,

K_{img} and V_{img} are cached for all L layers at once at the beginning of decoding, as defined below:

$$\begin{aligned}
 \text{For } l \in [1, 2, \dots, L] : \\
 K_{\text{img}}^{(l)} &= X_{\text{img}}^{(l)} \cdot W_K^{(l)}, \quad V_{\text{img}}^{(l)} = X_{\text{img}}^{(l)} \cdot W_V^{(l)}
 \end{aligned} \tag{8}$$

Using the cached K_{img} and V_{img} , text tokens can be generated autoregressively in the same manner as conventional retention mechanisms. This process is defined as follows:

$$\begin{aligned}
 S_n &= \gamma \cdot S_{n-1} + k_n^\top \cdot v_n \\
 o_{\text{text}, n} &= q_n \cdot S_n \in \mathbb{R}^{1 \times d_{\text{model}}} \\
 o_{\text{img}, n} &= \text{softmax} \left(\frac{q_n \cdot K_{\text{img}}^\top}{\sqrt{d_k}} \right) \cdot V_{\text{img}} \\
 \text{ARMF}(x_n) &= o_{\text{text}, n} + o_{\text{img}, n}, \quad n = 1, \dots, |x|
 \end{aligned} \tag{9}$$

Thus, the per-step decoding cost is $O(N_I)$ and does not grow with the generated text length N_T ; in our setting where N_I is fixed, this is effectively $O(1)$ per step. Consequently, the total decoding complexity is reduced from $O(N_T^2 + N_I N_T)$ to $O(N_I N_T)$, which is linear in N_T .

4.2. Multi-Scale ARMF (MARMF) with Layer-wise Gamma Scaling

Instead of using a uniform γ across all layers as in the original Multi-scale Retention, our ARMF employs a layer-wise gamma scaling strategy. We define this process as follows:

$$\begin{aligned}
 \gamma_{l, h} &= 1 - \gamma_{\text{subtractor}} \left(1 - \frac{l}{L-1} \right) - e^{\text{linspace}(\log(1/32), \log(1/512), H)_h} \\
 \text{head}_h &= \text{ARMF}(X, \gamma_{l, h}) \\
 Y &= \text{Concat}(\text{head}_1, \dots, \text{head}_H) \\
 \text{MARMF}(X) &= YW_O
 \end{aligned} \tag{10}$$

Here, γ increases from smaller values in lower layers to larger values in upper layers, so lower layers emphasize local details while

deeper layers capture broader context. RetNet’s original block includes GroupNorm and a Swish-style gating mechanism; gating has been argued to be beneficial in attention-style models by adding non-linearity and sparsity and mitigating attention-sink behavior [39]. In DRetHTR, we omit these components to keep the architecture minimal and stable for line-level HTR, where the primary requirement is robust image–text alignment rather than maximizing long-range linguistic expressiveness.

Layer-wise gamma scaling design rationale This mechanism provides explicit sequential priors by exponentially decaying the influence of earlier tokens, thereby eliminating the need for softmax-based attention between text tokens. In RetNet, each retention head employs a decay factor γ that controls how much historical context is retained. By assigning smaller γ values to early decoder layers and progressively increasing them in deeper layers, we mimic the *inductive bias* observed in standard Transformers—where shallow layers capture local dependencies, and deeper layers attend to broader context. Crucially, this multi-scale retention allows different layers to specialise in *diverse-range* dependencies (local, mid-range, and global) without incurring the quadratic cost of standard attention. The layer-wise decay acts as a structural prior for sequence modeling, compensating for the loss of flexible attention weights with a principled and efficient mechanism.

Softmax-free token interactions Practically, we retain softmax attention only for interactions that involve image tokens, so that visual features can be aligned and injected into the decoding context. All text-to-text dependencies are modeled with softmax-free, recurrent retention, enabling linear-time decoding with reduced memory overhead. Despite removing softmax from text modeling, our γ -scaled retention remains competitive with full Transformers and scales robustly across datasets.

5. EVALUATION

5.1. IAM Handwriting Database

We conduct experiments on the line-level IAM dataset [12] using the standard Aachen split (IAM-A). Image sizes range from 100×45 to 2270×152 , with widths typically $4\text{--}15\times$ larger than heights. Text transcriptions range from 4 to 93 characters; about 90% of lines contain 30–60 characters, spanning 79 unique characters.

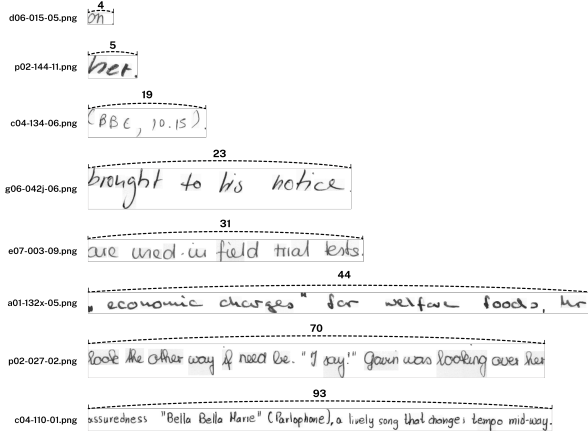


Fig. 3. Examples of text length variability in the IAM dataset, from short words to long sentences.

Orginal	installed correctly At least / ve done somethi
Vertical Padding	installed correctly At least / ve done somethi
Horizontal Padding	installed correctly At least / ve done somethi
Squeeze, Stretch	installed correctly At least / ve done somethi
Erosion	installed correctly At least / ve done somethi
Dilation	installed correctly At least / ve done somethi
Gaussian Noise Distortion	installed correctly At least / ve done somethi
Background Noise	installed correctly At least / ve done somethi

Fig. 4. Examples of the six augmentations applied to a handwriting image.

5.2. Synthetic Dataset for Pre-training

Our model was pre-trained with 17 million image-text pairs, providing visual diversity for general HTR tasks. To achieve this, we extracted millions of lines from the CC100 dataset [40], a corpus of 2 billion English text chunks. We randomly truncated these lines to fit the distribution of lengths of the IAM-A train dataset, ranging from a minimum length of 4 to a maximum length of 93 characters. Any emojis or characters not found in the dataset were replaced with an empty string for compatibility. After preparing the text, we produced the corresponding synthetic images using 11,954 different handwriting fonts from 1001 Fonts [41]. We assigned a randomly sampled font to each text line and rendered it as a text image in that font at a size of 100, which is close to the font size found in the IAM text lines.

5.3. Data Preprocessing and Augmentation

The handwriting text line images undergo a series of refined preprocessing steps. It starts by applying deslanting alone without contrast normalization. All images are resized to a constant height of 64 pixels while maintaining their original aspect ratio. However, this rescaling results in variable image widths. To perform mini-batch training, all resized images are padded with white pixels to have a uniform width of 2227 pixels. This padding is crucial, as it allows keeping the same input dimensions for the neural network. The final preprocessing step is the inversion of the pixels in the image, making the foreground (the handwritten stroke) close to 1 (white) and the background close to 0 (black). This enhances computational efficiency, increasing the prominence of features in the text while suppressing the numerical impact from the background. The dataset was augmented using six augmentation techniques, each applied with a 50% probability. These are random padding, squeezing & stretching, erosion, dilation, gaussian noise distortion, background noise. Examples of each augmentation are shown in Fig. 4.

5.4. Implementation Details

The base version of DRetHTR was configured with 12 layers, 768 hidden sizes, 12 heads, and a Position-wise Feed-Forward Network (PFF) of 3072 hidden sizes. The small version uses 4 layers, 1024 hidden sizes, 8 heads, and a 4096 hidden-size PFF. An EfficientNetV2-S is employed as the image embedder, with a layer-wise scaled gamma decay for both the image and text sequential priors. The optimizer uses AdamW with 10^{-3} weight decay and label smoothing ($\epsilon = 0.4$).

Table 3. Comparison of CER and WER between DRetHTR_{SMALL} and RetHTR_{SMALL} on different datasets.

Dataset	DRetHTR _{SMALL}		RetHTR _{SMALL}	
	CER ↓	WER ↓	CER ↓	WER ↓
IAM	4.49	13.05	4.45	12.93
IAM + Synth	2.97	9.13	3.01	9.20

For the learning rate, we used a cosine annealing schedule (10^{-4} to 10^{-6} restarting every 30 epochs). We set dropout rates of 0.3 for retention and PFF layers and 0.1 for embeddings. The pre-training on synthetic data was run on 8x NVIDIA A100 (80 GB) GPUs with a batch size of 48, while fine-tuning used a batch size of 16. Single Precision (FP32) is used throughout training and inference, following the PyTorch defaults. To check the inference speed and memory consumption, we use a batch size of 128 with an A100 80GB GPU. The beam size for decoding is set to 10. Unless otherwise stated, all CER, speed, and memory results are averaged over five independent runs.

5.5. Ablation Studies

5.5.1. Decoder-Only vs Encoder-Decoder

We compare both of our Decoder-Only RetNet (DRetHTR) and Encoder-Decoder RetNet (RetHTR) architectures using a small 4-layer configuration. RetHTR also has a similarly configured 4-layer encoder with a 3072 hidden-size PFF. Without pre-training, RetHTR achieves slightly better results, as can be seen in Table 3. However, DRetHTR outperforms RetHTR with pre-training on the synthetic dataset. This highlights the strength of the decoder-only approach when data-rich pre-training is used. Moreover, Table 4 shows that the decoder-only architecture is 3.2x faster and uses 22 % less memory than the RetNet version. This aligns with the expectation that removing the encoder reduces computational cost.

Table 4. Model performance comparison showcasing memory and time usage for beam-search decoding on the IAM test set (Aachen split). We refer to our Transformer baselines as TrHTR (encoder-decoder) and DTrHTR (decoder-only), which are matched reimplementations of RetHTR/DRetHTR and distinct from TrOCR/DTrOCR. Times correspond to a single pass over the full IAM test set with beam size 6 and batch size 128 on a single NVIDIA A100 80GB GPU.

Model	Parameters	Memory↓ (beam=6)	Time↓ (beam=6)
DRetHTR _{SMALL}	73M	9GB	52.8s
RetHTR _{SMALL}	136M	11GB	170.4s
DTrHTR _{SMALL}	73M	15GB	64.5s
TrHTR _{SMALL}	133M	16GB	189.4s

5.5.2. Impact of different CNN feature extractors

As shown in Table 5, the ResNet50, used as a feature extractor of Kang *et al.* [24], obtained a CER of 4.57 with pre-training and 14.5 without pre-training in our decoder-only architecture. The ShallowCNN, introduced by Wick *et al.* [42], outperformed the ResNet50

Table 5. Comparison of CER (%) on IAM and IAM + Synth datasets for different CNN architectures.

CNN	CER (%) ↓	
	IAM	IAM + Synth
ResNet50	14.5	4.57
ShallowCNN	30.0	4.23
EfficientNetV2-S	4.49	2.97

on our DRetHTR with a CER of 4.23 in case of pre-training. However, EfficientNetV2-S excels both with and without synthetic pre-training. Trained only on IAM, it reaches a CER of 4.49 %, far below ResNet-50 (14.5 %) and the shallow CNN (30 %), suggesting its Mobile Inverted Bottleneck Convolution (MBCConv) + Squeeze and Excitation (SE) [35] design captures stroke cues even in low-data regimes. With pre-training, EfficientNetV2-S drops to 2.97 %, again ahead of ResNet-50 (4.57 %) and the shallow CNN (4.23 %). In practice the backbone progressively expanding receptive fields yield multi-scale, character-specific features that are crisper than those from ResNet’s early, heavy down-sampling, making EfficientNetV2 a strong drop-in visual backbone for decoder-only HTR.

5.5.3. Sequential Priors for Text

In RetNet, the decay factor $\gamma \in (0, 1)$ imposes a sequential prior that removes the need for softmax. The original recommendation sets γ close to 1 with mild head-wise variation, favoring long-range memorization. gRet further introduces a data-dependent γ via a temperature term τ , which also tends to keep γ near 1. While this mechanism can learn how dependency strength should decay with distance, it still treats dependencies largely at a global scale, even when only local evidence is needed, and this global bias can hinder performance on text lines where locality is often sufficient.

By contrast, a Transformer with softmax attention can flexibly emphasize either local or global dependencies as needed. In our Decoder-only Transformer for HTR (DTrHTR), we observe that attention often skews local rather than uniformly global. As shown in Fig. 5a, the first layer concentrates on near-diagonal entries (the token and its neighbors), while deeper layers progressively broaden their receptive field. To mirror this behavior with retention, we assign smaller γ in early decoder layers and increase it in deeper layers. The corresponding D -matrix visualizations for different γ values are provided in Fig. 5b.

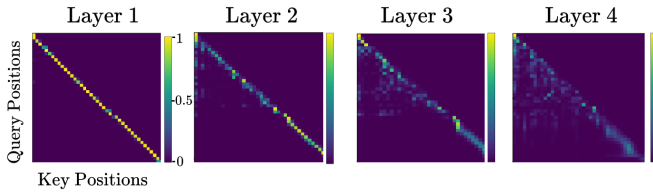
Table 6 summarizes several γ schedules and their CERs, evaluated on DRetHTR_{SMALL} with an EfficientNetV2-S image embedder on the IAM Aachen split without the synthetic set, using $\gamma_{\text{subtractor}} = 0.86$ tuned on IAM-val. Simply lowering all heads’ γ to emphasize locality already improves over the original schedule. Introducing *layer-wise* variation yields a further gain, matching the *Transformer with softmax* at **4.49 % CER** while keeping text–text interactions *softmax-free*.

5.5.4. Sequential priors for Image

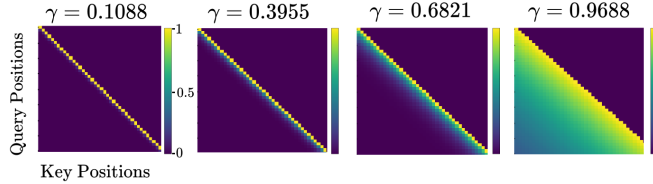
As introduced in [34], adding spatial priors in Vision Transformers can provide a boost in performance. The default implementation here applies softmax attention between image tokens with no spatial priors. For the CNN image embedder, the feature map is compressed into a single dimension. Thus, a simple Euclidean distance-based

Table 6. Ablation of γ scheduling on IAM (Aachen split) with an EfficientNetV2-S image encoder. All CER values are measured on the test set of Aachen split. Layer-wise γ scaling (last row) matches the Transformer’s CER (4.49 %) while retaining RetNet’s *softmax-free* token interactions, enabling *linear-time, linear-memory* decoding. See Fig. 5a for the local→global progression that motivates the schedule.

Strategy	Gamma Value	CER ↓
Original	$\gamma = 1 - e^{\text{linspace}(\log 1/32, \log 1/512, H)}$	4.65
+ Data dependent gating	$\gamma = \text{sigmoid}(XW_\gamma)^{1/\tau}$	4.66
+ Small Gamma Only	$\gamma = 1 - \gamma_{\text{subtractor}} - e^{\text{linspace}(\log 1/32, \log 1/512, H)}$	4.60
+ Head-wise Gamma Scaling	$\gamma_h = (1 - \gamma_{\text{subtractor}} - \frac{1}{32}) + \frac{h-1}{H-1} \gamma_{\text{subtractor}}$	4.51
+ Layer-wise Gamma Scaling	$\gamma_l = 1 - \gamma_{\text{subtractor}} \left(1 - \frac{l}{L-1}\right) - e^{\text{linspace}(\log(1/32), \log(1/512), H)}$	4.49
Transformer with Softmax	–	4.49



(a) Self-attention matrices of DTrHTR across decoder layers: shallow layers concentrate near the diagonal (local context), while deeper layers broaden to longer-range context.



(b) Retention decay matrices D for the corresponding γ settings, showing how smaller γ emphasizes locality and larger γ increases memory, as in the proposed layer-wise schedule.

Fig. 5. Local-to-global progression and its retention mimic. (a) In the Transformer baseline (DTrHTR), attention naturally shifts from local to broader context with depth. (b) By assigning smaller γ to early decoder layers and larger γ to deeper layers, retention reproduces a similar progression without softmax for text–text interactions (cf. Table 6).

prior is added bidirectionally. Notably, this adjustment yielded better performance with a substantially faster convergence speed.

Tokenization Table 8 compares Character-Level and Byte Pair Encoding (BPE) tokenization methods for both zero-shot and fine-tuned scenarios. BPE yields a better zero-shot performance for CER and WER than Character-Level tokenization. However, when fine-tuning with the IAM dataset, Character-level tokenization yields a better CER, while Byte Pair Encoding results in a better WER.

5.6. Qualitative error analysis on IAM

Figure 6 plots the three IAM lines with the highest CER after excluding samples whose ground truth is faulty. Lines 1–2 are heavily cursive, with strokes so entangled that even humans struggle, so large errors are unsurprising. Line 3 is more telling: the image is entirely uppercase, yet DRetHTR writes the sentence mostly in lowercase,

Table 7. Effect of Sequential Priors on image tokens. RetNet’s temporal decay is applied bidirectionally, and layer-wise gamma scaling is added to it.

Sequential Priors for Image	CER ↓
Priors only on text	4.49
+ RetNet’s temporal decay on image	4.41
+ Layer-wise gamma scaling on image	4.35

Table 8. Comparison of Character Error Rate (CER) and Word Error Rate (WER) of DRetHTR_{BASE} for different tokenization methods in both zero-shot and fine-tuned scenarios on the IAM test set (Aachen split). BPE uses a vocabulary size 500. BPE improves zero-shot via shorter sequences; character-level wins after fine-tuning due to precise character mapping in HTR.

Tokenization	CER (%) ↓	WER (%) ↓
<i>Zero-shot Performance</i>		
Character-Level	11.72	42.09
BPE $ \mathcal{V} = 500$	9.12	19.87
<i>Fine-tuned on IAM-A</i>		
Character-Level	2.26	6.55
BPE $ \mathcal{V} = 500$	2.36	4.81

capitalizing only the last two words. This shows the decoder isn’t just copying glyph shapes; it invokes RetNet’s language prior to produce the more natural casing for English prose.

5.7. Generalization beyond IAM

We evaluate DRetHTR on three additional benchmarks beyond IAM—RIMES (French) [13], READ-2016 (German) [14], and Bentham (English) [15]—using the same preprocessing and decoding settings as IAM and without external lexicons (Table 9). RIMES consists of modern French administrative mail and faxes collected from over 1,300 volunteers between approximately 2006 and 2011. READ-2016 provides a historical German benchmark featuring archival council minutes from 1470–1805, characterized by significant background noise and Early Modern German script. Bentham comprises English philosophical manuscripts written primarily between 1760 and 1832, featuring the challenging, idiosyncratic handwriting of a single author. Together, these benchmarks test

carrying it into effect, and a subordinate

CER 41.86
Predicted correjungise into affect , and a professional
Actual carrying it into effect , and a subordinate

thirst.

CER 37.50
Predicted this).
Actual thirst .

SUPPOSE, TO MEET ME FOR SUPPER SOMEWHERE ? " SHE HAD

CER 33.96
Predicted suppose , to meet me for supper supper comentries ? " SHE HAD
Actual suppose , to meet me for supper somewhere ? " she had

Fig. 6. The three hardest IAM lines for DRetHTR (highest CER), excluding faulty labels.

Table 9. Test CER (%) on four benchmarks. DRetHTR is pre-trained on the English synthetic dataset and fine-tuned separately on IAM, RIMES, READ-2016, and Bentham, and evaluated on the corresponding official test sets (IAM Aachen split, RIMES test set, READ-2016 test set, and Bentham test set).

Method	IAM	RIMES	READ-2016	Bentham
DRetHTR _{BASE} (ours)	2.26	1.81	4.21	3.46
DTrOCR [9]	2.38	—	—	—
Diaz <i>et al.</i> [25]	2.75	1.99	—	—
Retsinas <i>et al.</i> [43]	4.22	2.70	—	—
Wang <i>et al.</i> [44]	6.40	2.70	—	—
Coquenet <i>et al.</i> [45]	4.45	1.91	3.59	—
Abdallah <i>et al.</i> [46]	7.80	—	—	7.10

model robustness against high writer variability, archival degradation, and centuries of linguistic evolution.

As shown in Table 9, DRetHTR matches or surpasses strong CTC baselines on RIMES and Bentham, and remains competitive on READ-2016. This indicates that our decoder-only RetNet is not specialized to IAM but generalizes robustly across languages, scripts, and writing styles.

5.8. Comparative Inference Time and Memory Efficiency

The main benefits of RetNet are short inference time and low memory requirements. As seen in Table 10, in our implementation, RetNet outperforms Transformer in every evaluated aspect, including inference time, memory consumption, and CER. With BPE, which makes the total tokens less than character-level tokenization, it achieves 1.5x faster inference. Additionally, compared to the TrOCR models¹, our approach provides better performance with fewer parameters but significantly improves the inference speed. The memory consumption is measured by the difference in peak allocated memory before and after decoding one batch. For the other settings, see Section 5.4.

5.9. Beam Search Efficiency of RetNet

Beam search magnifies decoding-time overheads because all decoder states must be maintained and updated for beam size of candidate

¹This code version is from the Hugging Face documentation: https://huggingface.co/docs/transformers/model_doc/trocr

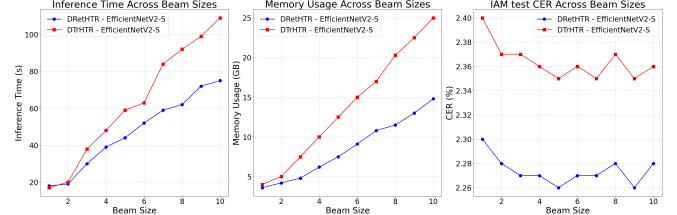


Fig. 7. Beam-size scaling on the IAM Aachen test set: end-to-end inference time (left), peak memory (middle), and test CER (right) for DRetHTR vs. DTTrHTR. DRetHTR scales more favorably with beam size because of fixed-size recurrent states, whereas KV-cached decoding incurs beam-dependent cache growth and cache reindexing after beam pruning. CER generally improves with larger beams up to $B = 5$, after which it fluctuates slightly while decoding cost continues to grow with B .

partial transcriptions in parallel. In a KV-cached Transformer, each beam stores a growing history of keys and values for every layer, and beam pruning requires reindexing these caches at every step. It also allocates temporary tensors when appending new keys/values, making decoding increasingly memory- and bandwidth-bound as beam size grows. In contrast, RetNet’s recurrent form maintains a fixed-size per-layer state for each beam and updates it in-place, avoiding sequence-length-dependent KV caches and reducing cache-management overhead.

From an asymptotic FLOP perspective (Table 2), a KV-cached Transformer requires $O(nd)$ work per decoding step, whereas RetNet’s recurrent update scales as $O(d^2)$. This suggests that recurrent decoding is expected to be FLOP-favorable mainly when the generated length n exceeds the model width d , as in long-sequence settings. However, wall-clock decoding on GPUs is not determined by FLOPs alone: cache growth, reindexing, and memory traffic can dominate runtime under beam search. Empirically, we find that RetNet remains faster and more memory efficient even on IAM, where sequences are relatively short ($n < d$), because the Transformer’s per-beam KV cache and its associated management overhead grow with both n and beam size B , while RetNet’s recurrent state is fixed-size and beam-friendly.

Table 12 summarizes the dominant per-layer storage for both approaches. For DTTrHTR_{BASE} ($d=768$, $H=12$) and a representative maximum decoding length $N = 94$, RetNet stores $B d^2/H$ elements per layer, whereas the Transformer stores $2 B N d$ elements for KV caching. Figure 7 reports end-to-end latency and peak memory across beam sizes on IAM Aachen split test set, showing that DRetHTR scales more favorably as the beam size increases. Finally, we observe that recognition accuracy typically saturates at moderate beams (around $B=5$), indicating that most remaining errors are dominated by visual/model ambiguity rather than insufficient search. We evaluate up to $B=10$ for consistency with TrOCR; however, in our setting the decoder uses character-level tokenization or a small BPE vocabulary of 500, which yields a more peaked next-token distribution and a smaller branching factor than GPT-2 tokenization. Consequently, larger beams provide limited additional diversity and do not materially improve CER, while still increasing decoding cost.

6. LIMITATIONS

A central design choice in DRetHTR is to retain softmax only where it mediates image–text fusion, while modeling text–text dependent-

Table 10. Comparative inference efficiency of RetNet, Transformer, and TrOCR models on the IAM test set (Aachen split). All times and memory values are measured for decoding the full IAM test set with the specified tokenization and beam size, using batch size 128 on a single NVIDIA A100 80 GB GPU.

Model	Params	Tokenization	Total Tokens	Inference Time ↓	Memory ↓	CER ↓
DRetHTR_{BASE}	107M	Character Level	442,832	123s	22.14GB	2.26
DTrHTR_{BASE}	107M	Character Level	442,832	233s	36.25GB	2.35
DRetHTR_{SMALL}	73M	Character Level	442,832	67s	14.5GB	2.97
DTrHTR_{SMALL}	73M	Character Level	442,832	110s	25.1GB	2.98
DRetHTR_{SMALL}	74M	BPE $ \mathcal{V} = 500$	49,574	44s	14.9GB	3.01
DTrHTR_{SMALL}	74M	BPE $ \mathcal{V} = 500$	49,574	69s	23.9GB	3.01
TROCR_{SMALL}	62M	BPE(GPT-2) $ \mathcal{V} = 50, 257$	31,959	310s	9.1GB	4.22
TROCR_{BASE}	334M	BPE(GPT-2) $ \mathcal{V} = 50, 257$	31,959	1717s	12.3GB	3.42
TROCR_{LARGE}	558M	BPE(GPT-2) $ \mathcal{V} = 50, 257$	31,959	2725s	13.5GB	2.89

Table 11. Comparison of HTR models: parameters, architecture, training data, external language model (LM) usage, and CER on the IAM test set (Aachen split). Abbrev.: Syn = synthetic data; Int. = internal data; Tx = Transformer; EN-V2 = EfficientNetV2. For architectures, $L/h/d$ denote the number of blocks (layers), attention heads per block, and embedding dimension (e.g., $L24, h16, d1024$ means 24 layers, 16 heads, 1024-dim embeddings).

Model	Params	Encoder	Decoder	Train	LM	CER ↓
DAN [44]	≈2.18M	23Conv+GRU	GRU, L1/d256	IAM	No	6.40
Wick <i>et al.</i> [42]	≈22M	3Conv + Tx, L3/h8/d512	Bidi Tx, L3/h8/d512	IAM	No	5.67
Michael <i>et al.</i> [47]	≈1.8M	3Conv+3BLSTM, d256	Attn-LSTM, L1/d256	IAM	No	4.87
HTR-VT [26]	53.5M	ResNet18 + Tx-Enc, L4/h6/d768	CTC	IAM	No	4.7
Kang <i>et al.</i> [24]	100M	Tx w/ResNet50, L4/h8/d1024	Tx, L4/h8/d1024	Syn+IAM	No	4.67
VAN [45]	2.7M	18 VGG-style Conv	1×LSTM d256 + CTC	IAM	No	4.45
Puigcerver [5]	≈8.3M	5Conv	5×BiLSTM d256 + CTC	IAM	Yes	4.4
Bluche and Messina [22]	0.75M	GCRNN, 6Conv+2BiLSTM, d128	CTC	Syn+IAM	No	3.20
TrOCR _{LARGE} [31]	558M	BEiT _{LARGE} , L24/h16/d1024	RoBERTa _{LARGE} , L12/h16/d1024	Syn+IAM	No	2.89
Diaz <i>et al.</i> [25]	1.5M	SelfAttn, L16/h4/d256	CTC	Int.+IAM	Yes	2.75
DTrOCR [9]	105M	–	GPT-2, L12/h12/d768	Syn+IAM	No	2.38
DRetHTR_{SMALL} (ours)	73M	–	RetNet w/EN-V2, L4/h8/d1024	IAM	No	4.35
DRetHTR_{SMALL} (ours)	73M	–	RetNet w/EN-V2, L4/h8/d1024	Syn+IAM	No	2.97
DRetHTR_{BASE} (ours)	107M	–	RetNet w/EN-V2, L12/h12/d768	Syn+IAM	No	2.26

Table 12. Dominant per-layer state size for beam-search decoding. d is the model dimension, H the number of heads, N the decoded length, and B the beam size. Example element counts use $d=768$, $H=12$, $N\approx94$, and $B=10$ (DTrHTR_{BASE}). RetNet’s state is fixed-size in N , while KV caching scales linearly with N .

Decoding Method	Memory per Layer	Number of Elements
Recurrent (RetNet)	$B d^2/H$	0.49M
KV-Cached Transformer	$2 B N d$	2.88M

cies via softmax-free retention with sequential priors. This design delivers clear efficiency gains and, in our experiments, even improves recognition accuracy relative to the decoder-only Transformer baseline (DTrHTR). In particular, DTrHTR normalizes each text query over a single key set that mixes image and text tokens, so visual evidence and linguistic context compete within one probability simplex. By contrast, DRetHTR effectively restricts softmax normalization for a text query to image keys, while handling text–text interactions separately through retention with a structured decay. The observed

improvement of DRetHTR over DTrHTR is therefore consistent with the hypothesis that joint softmax over all keys can dilute the model’s ability to concentrate probability mass on the most relevant image tokens, especially under visually ambiguous handwriting. However, our experiments do not provide a controlled ablation that isolates (i) the presence of softmax itself, (ii) the scope of its normalization (all tokens vs. modality-specific subsets), and (iii) its interaction with retention-style sequential priors.

In addition, our evaluation is centered on line-level benchmarks with moderate sequence lengths, and thus does not fully probe the regime $n \gg d$ where retentive decoding is expected to provide its strongest computational advantage over KV-cached attention. Finally, we do not systematically study alignment stability under very long autoregressive decoding, where accumulated errors can lead to *attention drift* and degrade visual–text correspondence.

7. FUTURE WORK

A natural next step is to explicitly factorize the normalization for text queries, e.g., by computing separate attention distributions over image

keys and text keys (or by using a gated mixture of the two), and then comparing these variants with and without retention-based sequential priors for text–text dependencies. Such an analysis could clarify whether DRetHTR benefits primarily from restricting cross-modal competition in a single softmax normalization, from the structured inductive bias introduced by layer-wise gamma scaling, or from the interaction between the two.

Beyond this, future work should stress-test retentive decoding on substantially longer sequences to characterize efficiency and accuracy as n grows into the $n \gg d$ regime, and to quantify when recurrent decoding becomes decisively advantageous in practice. Mitigating attention drift for long-form decoding is another important direction, potentially via alignment-regularized training objectives, lightweight alignment correction during decoding, or decoding strategies that explicitly monitor and stabilize image–text correspondence over time.

8. CONCLUSION

We introduced DRetHTR, a linear-time, linear-memory decoder-only handwritten text recognition model based on Retentive Networks, and demonstrated that softmax-free retentive decoding can achieve Transformer-level accuracy while substantially reducing inference cost. Across four benchmarks, DRetHTR attains state-of-the-art and competitive CER under consistent training and decoding settings, while lowering end-to-end decoding latency and peak memory relative to an equally-sized decoder-only Transformer baseline. These gains are enabled by two HTR-specific adaptations: ARMF preserves strong image–text alignment by retaining softmax attention at the modality interface while maintaining causal, recurrence-compatible text–text interactions; and layer-wise gamma scaling restores the local-to-global inductive bias of Transformers by progressively expanding the effective retention horizon with depth. Overall, our results establish retention as a practical alternative to KV-cached attention for HTR, combining competitive accuracy with substantially improved decoding efficiency.

9. REFERENCES

- [1] Joe Nockels, Paul Gooding, Sarah Ames, and Melissa Terras, “Understanding the application of handwritten text recognition technology in heritage contexts: a systematic review of transkribus in published research,” *Archival Science*, vol. 22, no. 3, pp. 367–392, 2022.
- [2] Guenter Muehlberger et al., “Transforming scholarship in the archives through handwritten text recognition,” *Journal of Documentation*, vol. 75, no. 5, pp. 954–976, 2019.
- [3] Thomas Plötz and Gernot A. Fink, “Markov models for offline handwriting recognition: a survey,” *International Journal on Document Analysis and Recognition (IJDAR)*, vol. 12, no. 4, pp. 269–298, 2009.
- [4] Christopher Tensmeyer, Curtis Wigington, Brian Davis, Seth Stewart, Tony Martinez, and William Barrett, “Language model supervision for handwriting recognition model adaptation,” in *2018 16th International Conference on Frontiers in Handwriting Recognition (ICFHR)*, 2018, pp. 133–138.
- [5] Joan Puigcerver, “Are multidimensional recurrent layers really necessary for handwritten text recognition?,” in *2017 14th IAPR International Conference on Document Analysis and Recognition (ICDAR)*, 2017, vol. 01, pp. 67–72.
- [6] Patrick Doetsch, Michal Kozielski, and Hermann Ney, “Fast and robust training of recurrent neural networks for offline handwriting recognition,” in *2014 14th International Conference on Frontiers in Handwriting Recognition (ICFHR)*, 2014, pp. 279–284.
- [7] Alex Graves, Santiago Fernández, Faustino Gomez, and Jürgen Schmidhuber, “Connectionist temporal classification: labelling unsegmented sequence data with recurrent neural networks,” in *International Conference on Machine Learning (ICML)*, 2006, pp. 369–376, ACM.
- [8] Ashish Vaswani, Noam Shazeer, Niki Parmar, Jakob Uszkoreit, Llion Jones, Aidan N. Gomez, Łukasz Kaiser, and Illia Polosukhin, “Attention is all you need,” in *Advances in Neural Information Processing Systems (NeurIPS)*, 2017, vol. 30.
- [9] M Fujitake, “Dtrocr: Decoder-only transformer for optical character recognition,” in *IEEE/CVF Winter Conference on Applications of Computer Vision (WACV)*, 2024, pp. 8010–8020.
- [10] Alec Radford et al., “Language models are unsupervised multi-task learners,” 2019.
- [11] Yutao Sun, Li Dong, Shaohan Huang, Shuming Ma, Yuqing Xia, Jilong Xue, Jianyong Wang, and Furu Wei, “Retentive network: A successor to transformer for large language models,” 2023, preprint.
- [12] Urs-Viktor Marti and Horst Bunke, “The iam-database: an english sentence database for offline handwriting recognition,” *International Journal on Document Analysis and Recognition (IJDAR)*, vol. 5, no. 1, pp. 39–46, 2002.
- [13] Emmanuèle Grosicki, Matthieu Carré, Edouard Geoffrois, Emmanuel Augustin, Françoise Preteux, and Ronaldo Messina, “Rimes, complete,” Mar. 2024.
- [14] A.H. Toselli, V. Romero, M. Villegas, E. Vidal, and J.A. Sánchez, “Htr dataset icfhr 2016,” Feb. 2018.
- [15] Joan Andreu Sánchez, “Bentham dataset r0,” Jan. 2016.
- [16] Nadir Farah, Labiba Souici, Lotfi Farah, and Mokhtar Sellami, “Arabic words recognition with classifiers combination: An application to literal amounts,” in *Artificial Intelligence: Methodology, Systems, and Applications*. 2004, pp. 420–429, Springer.
- [17] Alex Graves et al., “Offline handwriting recognition with multi-dimensional recurrent neural networks,” in *Advances in Neural Information Processing Systems (NeurIPS)*, 2008, vol. 21.
- [18] Théodore Bluche, “Joint line segmentation and transcription for end-to-end handwritten paragraph recognition,” in *Advances in Neural Information Processing Systems (NeurIPS)*, 2016, pp. 838–846.
- [19] F. Zamora-Martínez, V. Frinken, S. España-Boquera, M.J. Castro-Bleda, A. Fischer, and H. Bunke, “Neural network language models for off-line handwriting recognition,” *Pattern Recognition*, vol. 47, no. 4, pp. 1642–1652, 2014.
- [20] Curtis Wigington, Seth Stewart, Brian Davis, Bill Barrett, Brian Price, and Scott Cohen, “Data augmentation for recognition of handwritten words and lines using a cnn-lstm network,” in *2017 14th IAPR International Conference on Document Analysis and Recognition (ICDAR)*, 2017, pp. 639–645.
- [21] Vu Pham, Théodore Bluche, Christopher Kermorvant, and Jérôme Louradour, “Dropout improves recurrent neural networks for handwriting recognition,” in *2014 14th International Conference on Frontiers in Handwriting Recognition (ICFHR)*, 2014, pp. 285–290.

[22] Théodore Bluche and Ronaldo Messina, “Gated convolutional recurrent neural networks for multilingual handwriting recognition,” in *2017 14th IAPR International Conference on Document Analysis and Recognition (ICDAR)*, 2017, pp. 646–651.

[23] Fenfen Sheng, Zhineng Chen, and Bo Xu, “Nrtr: A no-recurrence sequence-to-sequence model for scene text recognition,” in *2019 International Conference on Document Analysis and Recognition (ICDAR)*, 2019, pp. 781–786.

[24] Lei Kang, Pau Riba, Marçal Rusiñol, Alicia Fornés, and Mauricio Villegas, “Pay attention to what you read: Non-recurrent handwritten text-line recognition,” *Pattern Recognition*, vol. 129, pp. 108766, 2022.

[25] Daniel Hernandez Diaz et al., “Rethinking text line recognition models,” *arXiv preprint arXiv:2104.07787*, vol. abs/2104.07787, 2021, preprint.

[26] Yuting Li, Dexiong Chen, Tinglong Tang, and Xi Shen, “Htr-vt: Handwritten text recognition with vision transformer,” *Pattern Recognition*, vol. 158, pp. 110967, 2025.

[27] Martin Mayr, Katharina Neumeier, Julian Krenz, Simon Bürky, Florian Kordon, Mathias Seuret, Jochen Zöllner, Fei Wu, Andreas Maier, and Vincent Christlein, “Data-efficient handwritten text recognition of diplomatic historical text,” *Multimedia Tools and Applications*, vol. 84, pp. 39107–39122, 2025.

[28] Killian Barrere, Yann Soullard, Aurélie Lemaitre, and Bertrand Couasnon, “A light transformer-based architecture for handwritten text recognition,” in *International Workshop on Document Analysis Systems (DAS)*, 2022, pp. 275–290.

[29] Killian Barrere et al., “Training transformer architectures on few annotated data: an application to historical handwritten text recognition,” *International Journal on Document Analysis and Recognition (IJDAR)*, 2024.

[30] Christoph Wick, Jochen Zöllner, and Tobias Grüning, “Rescorning sequence-to-sequence models for text line recognition with ctc-prefixes,” in *Document Analysis Systems (DAS) 2022*, Seiichi Uchida, Elisa Barney, and Véronique Egliv, Eds. 2022, vol. 13227 of *Lecture Notes in Computer Science*, pp. 260–274, Springer, Cham.

[31] Minghao Li, Tengchao Lv, Jingye Chen, Lei Cui, Yijuan Lu, Dinei Florencio, Cha Zhang, Zhoujun Li, and Furu Wei, “Trocr: Transformer-based optical character recognition with pre-trained models,” in *AAAI Conference on Artificial Intelligence (AAAI)*, 2023.

[32] Haoyang Li, Yiming Li, Anxin Tian, Tianhao Tang, Zhanchao Xu, Xuejia Chen, Nicole Hu, Wei Dong, Qing Li, and Lei Chen, “A survey on large language model acceleration based on kv cache management,” *Transactions on Machine Learning Research*, 2025.

[33] Yutao Sun, Li Dong, Yi Zhu, Shaohan Huang, Wenhui Wang, Shuming Ma, Quanlu Zhang, Jianyong Wang, and Furu Wei, “You only cache once: Decoder-decoder architectures for language models,” in *Advances in Neural Information Processing Systems (NeurIPS)*, 2024, pp. 7339–7361.

[34] Qihang Fan, Huabo Huang, Mingrui Chen, Hongmin Liu, and Ran He, “Rmt: Retentive networks meet vision transformers,” in *IEEE/CVF Conference on Computer Vision and Pattern Recognition (CVPR)*, 2024, pp. 5641–5651.

[35] Mingxing Tan and Quoc V. Le, “Efficientnetv2: Smaller models and faster training,” in *International Conference on Machine Learning (ICML)*, 2021.

[36] Jia Deng, Wei Dong, Richard Socher, Li-Jia Li, Kai Li, and Li Fei-Fei, “Imagenet: A large-scale hierarchical image database,” in *2009 IEEE Conference on Computer Vision and Pattern Recognition (CVPR)*, 2009, pp. 248–255.

[37] Kaiming He, Xiangyu Zhang, Shaoqing Ren, and Jian Sun, “Deep residual learning for image recognition,” in *IEEE/CVF Conference on Computer Vision and Pattern Recognition (CVPR)*, 2016, pp. 770–778.

[38] Jimmy Lei Ba, Jamie Ryan Kiros, and Geoffrey E. Hinton, “Layer normalization,” 2016, preprint.

[39] Zihan Qiu, Zekun Wang, Bo Zheng, Zeyu Huang, Kaiyue Wen, Songlin Yang, Rui Men, Le Yu, Fei Huang, Suozhi Huang, Dayiheng Liu, Jingren Zhou, and Junyang Lin, “Gated attention for large language models: Non-linearity, sparsity, and attention-sink-free,” in *Advances in Neural Information Processing Systems (NeurIPS)*, 2025.

[40] Guillaume Wenzek, Marie-Anne Lachaux, Alexis Conneau, Vishrav Chaudhary, Francisco Guzmán, Armand Joulin, and Edouard Grave, “CCNet: Extracting high quality monolingual datasets from web crawl data,” in *Proceedings of the Twelfth Language Resources and Evaluation Conference*, 2020, pp. 4003–4012.

[41] 1001 Fonts, “Handwritten fonts,” <https://www.1001fonts.com/handwritten-fonts.html>, Accessed: 2024-12-3.

[42] Christoph Wick, Jochen Zöllner, and Tobias Grüning, “Transformer for handwritten text recognition using bidirectional post-decoding,” in *2021 16th International Conference on Document Analysis and Recognition (ICDAR)*, 2021, pp. 112–126.

[43] George Retsinas, Giorgos Sfikas, Basilis Gatos, and Christophoros Nikou, “Best practices for handwritten text recognition,” in *International Workshop on Document Analysis Systems (DAS)*, 2022, pp. 247–259.

[44] Tianwei Wang, Yuanzhi Zhu, Lianwen Jin, Canjie Luo, Xiaoxue Chen, Yaqiang Wu, Qianying Wang, and Mingxiang Cai, “Decoupled attention network for text recognition,” in *Proceedings of the AAAI Conference on Artificial Intelligence*, 2020, vol. 34, pp. 12216–12224.

[45] Denis Coquenet, Clement Chatelain, and Thierry Paquet, “End-to-End Handwritten Paragraph Text Recognition Using a Vertical Attention Network,” *IEEE Transactions on Pattern Analysis & Machine Intelligence*, vol. 45, no. 01, pp. 508–524, Jan. 2023.

[46] Abdelrahman Abdallah, Mohamed Hamada, and Daniyar Nurseitov, “Attention-based fully gated cnn–bgru for russian handwritten text,” *Journal of Imaging*, vol. 6, no. 12, 2020.

[47] Johannes Michael, Roger Labahn, Tobias Grüning, and Jochen Zöllner, “Evaluating sequence-to-sequence models for handwritten text recognition,” *International Conference on Document Analysis and Recognition (ICDAR)*, pp. 1286–1293, 2019.

Appendix A. Connection between RetNet's Parallel and Recurrent Representation

To better understand the connection between parallel and recurrent equations, consider the following matrix operations:

1. Defining Q , K^\top , and V :

$$Q = \begin{bmatrix} q_1 \\ q_2 \\ q_3 \end{bmatrix}, \quad K^\top = \begin{bmatrix} k_1^\top & k_2^\top & k_3^\top \end{bmatrix}, \quad V = \begin{bmatrix} v_1 \\ v_2 \\ v_3 \end{bmatrix}.$$

2. Computing QK^\top and defining D :

$$QK^\top = \begin{bmatrix} q_1 k_1^\top & q_1 k_2^\top & q_1 k_3^\top \\ q_2 k_1^\top & q_2 k_2^\top & q_2 k_3^\top \\ q_3 k_1^\top & q_3 k_2^\top & q_3 k_3^\top \end{bmatrix}, \quad D = \begin{bmatrix} 1 & 0 & 0 \\ \gamma & 1 & 0 \\ \gamma^2 & \gamma & 1 \end{bmatrix}.$$

3. Computing the Retention Matrix:

$$(QK^\top) \odot D = \begin{bmatrix} q_1 k_1^\top & 0 & 0 \\ \gamma q_2 k_1^\top & q_2 k_2^\top & 0 \\ \gamma^2 q_3 k_1^\top & \gamma q_3 k_2^\top & q_3 k_3^\top \end{bmatrix}.$$

4. Final Retention Operation:

$$Y = \begin{bmatrix} q_1(k_1^\top v_1) \\ q_2(\gamma k_1^\top v_1 + k_2^\top v_2) \\ q_3(\gamma^2 k_1^\top v_1 + \gamma k_2^\top v_2 + k_3^\top v_3) \end{bmatrix} = \begin{bmatrix} q_1 S_1 \\ q_2 S_2 \\ q_3 S_3 \end{bmatrix}, \quad \text{where } S_n = \gamma S_{n-1} + k_n^\top v_n.$$

This formulation demonstrates the validity and flexibility of the retention mechanism.

Appendix B. Derivation of the Asymptotic Complexity for Each Inference Form

Appendix B.1 Vanilla Form of Transformer Total Computation

$$y_n = \text{softmax} \left(\frac{1}{\sqrt{d_k}} Q_n K_n^\top \right) V_n$$

- Where the shapes are:

$$Q_n : (n, d), \quad K_n^\top : (d, n), \quad V_n : (n, d)$$

1. Compute $Q_n K_n^\top$

$$Q_n \cdot K_n^\top = \begin{bmatrix} q_{11} & q_{12} & \cdots & q_{1d} \\ q_{21} & q_{22} & \cdots & q_{2d} \\ \vdots & \vdots & \ddots & \vdots \\ q_{n1} & q_{n2} & \cdots & q_{nd} \end{bmatrix} \times \begin{bmatrix} k_{11} & k_{12} & \cdots & k_{1n} \\ k_{21} & k_{22} & \cdots & k_{2n} \\ \vdots & \vdots & \ddots & \vdots \\ k_{d1} & k_{d2} & \cdots & k_{dn} \end{bmatrix}$$

- Total Computations: $n \times d \times n = n^2 \times d$ multiplications, $n^2 - 1$ additions.

2. Compute $\text{softmax} \left(\frac{1}{\sqrt{d_k}} Q_n K_n^\top \cdot \text{Mask} \right) \times V_n$:

$$\text{attn} \times V_n =$$

$$\begin{bmatrix} \alpha_{11} & \alpha_{12} & \cdots & \alpha_{1n} \\ \alpha_{21} & \alpha_{22} & \cdots & \alpha_{2n} \\ \vdots & \vdots & \ddots & \vdots \\ \alpha_{n1} & \alpha_{n2} & \cdots & \alpha_{nn} \end{bmatrix} \times \begin{bmatrix} v_{n11} & v_{n12} & \cdots & v_{n1d} \\ v_{n21} & v_{n22} & \cdots & v_{n2d} \\ \vdots & \vdots & \ddots & \vdots \\ v_{nn1} & v_{nn2} & \cdots & v_{nnd} \end{bmatrix}$$

- Total Computations: $n \times d \times n = n^2 \times d$ multiplications, $n \times (d - 1)$ additions.

- Total Computations for Modified Form with Causal Mask:

$$(2n^2 \times d + n^2 - 1 + n \times (d - 1)),$$

which simplifies to $O(n^2 \times d)$.

- This process involves matrix multiplications across all n tokens for each generation step, resulting in $O(n^2 d)$ complexity per step.

The inefficiency is due to the causal nature of the decoder that redundantly recomputes the same attention weights for previously processed tokens.

Appendix B.2 Key-Value (KV) Cached Form

To address this inefficiency, instead of recomputing attention for all previous tokens, KV Caching stores the K and V from earlier steps. This modifies the computation as follows:

1 Key-Value Cached Form Total Computation:

$$y_n = \text{softmax} \left(\frac{1}{\sqrt{d_k}} q_n [K_{n-1}^\top | k_n^\top] \right) \begin{bmatrix} V_{n-1} \\ v_n \end{bmatrix}$$

- Where the shapes are: $q_n : (1, d)$

$$[K_{n-1}^\top | k_n^\top] : (d, n), \quad \begin{bmatrix} V_{n-1} \\ v_n \end{bmatrix} : (n, d)$$

2. Detailed Computation:

- Equation: $q_n [K_{n-1}^\top | k_n^\top] = q_n K_n^\top$
- Expanded as:

$$q_n \cdot [K_{n-1}^\top | k_n^\top] = \begin{bmatrix} k_{11} & k_{12} & \cdots & k_{1n} \\ k_{21} & k_{22} & \cdots & k_{2n} \\ \vdots & \vdots & \ddots & \vdots \\ k_{d1} & k_{d2} & \cdots & k_{dn} \end{bmatrix} \times \begin{bmatrix} q_{n1} & q_{n2} & \cdots & q_{nd} \end{bmatrix}$$

- Total Computations: $d \times n$ multiplications, $n - 1$ additions.

3. Output Computation:

$$\text{softmax} \left(\frac{1}{\sqrt{d_k}} q_n [K_{n-1}^\top | k_n^\top] \right) \begin{bmatrix} V_{n-1} \\ v_n \end{bmatrix} = \text{attn} \times V_n$$

- Expanded as:

$$\text{attn} \times V_n = \begin{bmatrix} v_{n11} & v_{n12} & \cdots & v_{n1d} \\ v_{n21} & v_{n22} & \cdots & v_{n2d} \\ \vdots & \vdots & \ddots & \vdots \\ v_{nn1} & v_{nn2} & \cdots & v_{nnd} \end{bmatrix} \times \begin{bmatrix} \alpha_{11} & \alpha_{12} & \cdots & \alpha_{1n} \\ \alpha_{21} & \alpha_{22} & \cdots & \alpha_{2n} \\ \vdots & \vdots & \ddots & \vdots \\ \alpha_{n1} & \alpha_{n2} & \cdots & \alpha_{nn} \end{bmatrix}$$

- Total Computations: $d \times n$ multiplications, $n - 1$ additions.

Total Computations for Key-Value Cached Form:

$$2dn + 2(n - 1), \text{ which is } O(nd).$$

- The overall computation is significantly reduced as it only computes the attention for the new token using cached keys and values.

Appendix B.3 RetNet's Recurrent Representation

RetNet can be considered a more advanced form of key-value caching. By discarding the softmax operation and introducing gamma decay, there is no longer a need to cache K and V separately. Instead, the network only needs to store the product $k_n^\top v_n$ at each step and update a recurrent state representation S_n by adding these values.

$$S_n = rS_{n-1} + k_n^\top v_n$$

$$y_n = q_n S_n$$

1. **Equation:** $S_n = rS_{n-1} + k_n^\top v_n$

- Matrix Multiplication: Simplifying to the last two dimensions $(d, 1) \cdot (1, d)$

$$\begin{aligned} k_n^\top \cdot v_n &= \begin{bmatrix} k_{n1} \\ k_{n2} \\ \vdots \\ k_{nd} \end{bmatrix} \times [v_{n1} \quad v_{n2} \quad \cdots \quad v_{nd}] \\ &= \begin{bmatrix} k_{n1}v_{n1} & k_{n1}v_{n2} & \cdots & k_{n1}v_{nd} \\ k_{n2}v_{n1} & k_{n2}v_{n2} & \cdots & k_{n2}v_{nd} \\ \vdots & \vdots & \ddots & \vdots \\ k_{nd}v_{n1} & k_{nd}v_{n2} & \cdots & k_{nd}v_{nd} \end{bmatrix} \end{aligned}$$

- Total Computations: d^2 multiplications, 0 additions.

2. **Equation:** $y_n = q_n S_n$

- Matrix Multiplication: Simplifying to the last two dimensions $(1, d) \cdot (d, d)$

$$\begin{aligned} y_n &= q_n \cdot S_n \\ &= [q_{n1} \quad q_{n2} \quad \cdots \quad q_{nd}] \times \begin{bmatrix} S_{n11} & S_{n12} & \cdots & S_{n1d} \\ S_{n21} & S_{n22} & \cdots & S_{n2d} \\ \vdots & \vdots & \ddots & \vdots \\ S_{nd1} & S_{nd2} & \cdots & S_{ndd} \end{bmatrix} \\ &= [y_{n1} \quad y_{n2} \quad \cdots \quad y_{nd}] \end{aligned}$$

- Total Computations: d^2 multiplications, $d - 1$ additions.

• **Total Computations for Recurrent Form:**

$$2d^2 + d - 1, \text{ which is } O(d^2).$$

Appendix C. Beam Search Decoding Memory Complexity

Appendix C.1 KV-Cached Decoding

Persistent Cache Storage:

For each layer, we store the keys and values for all decoded text tokens. Their typical shape is:

$$\text{Keys (or Values)} : (B, H, N, d_h)$$

Thus, the memory required per cache (key or value) is:

$$M_{\text{persistent, per cache}} = B \times H \times N \times d_h = B \times N \times d$$

Since both keys and values are stored, the total persistent memory is:

$$M_{\text{persistent}}^{\text{KV}} = 2BNd$$

Temporary Allocations during Concatenation:

At each decoding step t (where $t \leq N$), the model concatenates the new key and value $(B, H, 1, d_h)$ with the previous cache $(B, H, t - 1, d_h)$, resulting in a new cache of shape (B, H, t, d_h) .

The size of the temporary tensor created here for the concatenation is:

$$B \times H \times t \times d_h = B \times t \times d$$

In the worst case (at $t = N$), the temporary allocation per cache is:

$$M_{\text{temp, per cache}} \approx B \times N \times d$$

The total temporary memory required for both keys and values is:

$$M_{\text{temp}}^{\text{KV}} \approx 2BNd$$

Peak Memory Usage for KV-Cached Decoding:

The total peak memory, both persistent and temporary, can be expressed as:

$$M_{\text{KV}} \approx M_{\text{persistent}}^{\text{KV}} + M_{\text{temp}}^{\text{KV}} \approx 2BNd + 2BNd = 4BNd$$

Appendix C.2 Recurrent Decoding (RetNet Form)

Here, instead of storing the entire history, a fixed-size recurrent state is maintained. For each layer, assume the state has the shape:

$$(B, H, d_h, d_h)$$

Thus, the memory per layer is:

$$M_{\text{Recurrent}} \approx B \times H \times d_h \times d_h = B \times H \times \left(\frac{d}{H}\right)^2 = B \times \frac{d^2}{H}$$

Note that this memory usage does not grow with N .